Supporting Information

Tailoring of Nanoscale Porosity in Carbide-Derived Carbons for Efficient Hydrogen Storage

Yury Gogotsi[1*], Ranjan K. Dash[1], Gleb Yushin[1], Taner Yildirim[2], Giovanna Laudisio[3] & John E. Fischer[3]

[1]*Department of Materials Science and Engineering and A.J. Drexel Nanotechnology Institute, Drexel University, Philadelphia, PA, 19104, USA.* [2]*National Institute of Standards and Technology, Gaithersburg, MD 20899, USA.* [3]*Department of Materials Science and Engineering, University of Pennsylvania, Philadelphia, PA, 19104, USA.*

METHODS

Materials. The experimental setup and structure/composition of carbide powders for synthesis of CDC have been described elsewhere.[1] While many CDCs have been studied, providing a large volume of statistically reliable data, only data for CDC produced from boron carbide (B_4C), titanium carbide (TiC), zirconium carbide (ZrC) and silicon carbide (β-SiC) are referred to in this work. The particle sizes of the powders were 6 μm, 2 μm, 8 μm and 0.7 μm, respectively. The synthesis of CDC from these carbides was described in our previous publications.[1, 2] The starting material was placed into the quartz tube of a resistance furnace in a quartz boat. The furnace was then heated to the desired temperature (400 – 1200°C) under argon (BOC Gases, 99.998%) purge. Once the desired reaction temperature was reached, chlorine gas (BOC Gases, 99.5%) at 10-15 cm^3/min was passed through the tube furnace for 3 hours. After chlorination, the furnace was cooled to room temperature under argon purge. Hydrogen annealing was done using the same furnace at 600°C for 2 h. As shown by PGAA, chlorine trapped during the synthesis was a major contamination in the sample but its content decreases well below 1 at% after hydrogen treatment. Carbide forming metals may eventually be present in incompletely chlorinated samples, but their content in the TiC-CDC samples used to generate data of Fig. 3 was ~0.05 at.%.

Several other materials have been studied for comparison and independent verification of the results for CDC reported here. These include SWCNT from Rice University (TUBES@RICE) and open ended nanotubes from NanoCarbLab, Moscow (http://www.nanocarblab.com). According to the manufacturer, the latter sample was purified and activated by combination of acid treatment (HCl and HNO_3) and thermal oxidation in air flow. At the end, nanotubes were washed in water and dried in air flow at 140°C. Neutron powder diffraction performed at NIST indicated some graphite and nickel in that sample. Both of these SWNT materials stored less hydrogen than arc-discharge produced nanotubes oxidized at 350°C and containing metal oxide[3], so we report the latter in Fig. 3b as the best reliable result for SWCNT available to us. The MWCNT (10-20 nm diameter) reported in Fig. 3b come from Arkema, France, and were produced by a catalytic CVD technique. Deuturated MOF-5 samples with the molecular formula $Zn_4O_{13}C_{24}D_{12}$ were produced at NIST. Their structure and composition were confirmed by neutron scattering. The result that we obtained (Fig. 3a, 1.25 wt.% of H_2) is in good agreement with 1.3 wt.% reported for MOF-5 by Yaghi's group.[4]

Sorption analysis. Quantachrome Autosorb-1 was used for sorption analysis with argon as adsorbate at 77K as reported previously.[2] The SSA of the carbon material was calculated according to BET (Brunauer, Emmet, Teller) equation[5] and pore volume was calculated from argon adsorption using nonlocal density functional theory (NLDFT).[29] Weighted pore size of the carbons was defined as $\frac{\sum_{i=1}^{n} d_i . v_i}{\sum_{i=1}^{n} v_i}$, where d is pore size and v is pore volume. Gravimetric density of hydrogen (wt.%) was defined as $\left(\rho_{Hydrogen} . v_{Hydrogen} . 100\right)$, where $\rho_{Hydrogen}$ is the hydrogen density in g/cm^3, $v_{Hydrogen}$ is the volume of hydrogen adsorbed at ~760 mm of Hg per unit mass of CDC, in cm^3/g. Results of all measurements have been summarized in Supplement 1.

Hydrogen sorption isotherms were collected using Quantachrome Autosorb-1 at 77K as described in Quantachrome's technotes.[6] This technique has been widely used to study hydrogen sorption on a variety of carbons, including activated carbons[7] and nanotubes[3], and it enables comparison with literature data. Its advantage is in recording the full sorption/desorption cycle, which decreases possibility of error and shows if any irreversible sorption occurs. The gravimetric and volumetric densities of stored hydrogen were based on sample mass after degassing at 300ºC in vacuum and on the calculated specific weight of CDC derived from carbides. Independent measurements were conducted on selected samples at Quantachrome's laboratory to validate those performed at Drexel University. These were conducted on TiC- and ZrC-CDC using Autosorb-1 and Nova instruments and demonstrated excellent agreement with our data reported in this article. This also allows us to comfortably compare our results with those reported for SWCNT in ref. [3] authored by Quantachrome researchers (see Fig. 3b). Sieverts apparatus measurements were also performed at NIST to compare CDC with SWCNT and MOF-5 samples.

References:

(1) Dash, R. K.; Nikitin, A.; Gogotsi, Y., *Microporous and Mesoporous Materials* **2004,** 72, 203-208.
(2) Dash, R. K.; Yushin, G.; Gogotsi, Y., *Microporous and Mesoporous Materials* **in press, 2005**.
(3) Anson, A.; Callejas, M. A.; Benito, A. M.; Maser, W. K.; Izquierdo, M. T.; Rubio, B.; Jagiello, J.; Thommes, M.; Parra, J. B.; Martınez, M. T., *Carbon* **2004,** 42, 1243–1248.
(4) Rowsell, J.; Millward, A.; Park, K.; Yaghi, O. M., *J. Am. Chem. Soc.* **2004,** 126, 5666-5667.
(5) Brunauer, S.; Emmett, P.; Teller, E., *J. Am. Chem. Soc.* **1938,** 60, 309–319.
(6) *Powder Technote 37, Quantachrome Corporation, 1900 Corporate Drive, Boynton Beach, FL 33426 USA, < http://www.quantachrome.com >.*
(7) Jagiello, J.; Thommes, M., *Carbon* **2004,** 42, 1227-1232.

Supplement 1. CDC synthesis conditions and results of sorption measurements.

Synthesis conditions		Analysis of 77K argon sorption isotherms			Hydrogen uptake at 77K, 1 atm pressure, cc/g (wt%)	Hydrogen uptake per SSA, $\frac{wt\%.g}{m^2}.10^3$
Metal carbide	Chlorination temperature, ^oC	BET SSA, m^2/g	Pore size, nm	Pore volume, cc/g		
TiC	400	1199	0.74	0.54	179 (1.61)	1.34
TiC	600	1058	0.67	0.47	255 (2.29)	2.17
TiC	800	1566	0.92	0.82	284 (2.55)	1.63
TiC	1200	1714	1.42	0.93	171 (1.54)	0.90
TiC	400*	1113	0.68	0.51	269 (2.42)	2.17
TiC	800*	1943	1.00	0.94	336 (3.02)	1.55
ZrC	400	494	0.75	0.23	125 (1.12)	2.27
ZrC	600	859	0.80	0.48	180 (1.62)	1.88
ZrC	800	1342	0.83	0.61	214 (1.92)	1.43
ZrC	1000	1499	1.21	0.72	207 (1.86)	1.24
ZrC	1200	1857	1.41	0.91	220 (1.98)	1.07
ZrC	400*	1073	0.72	0.51	217 (1.95)	1.82
ZrC	600*	1388	0.97	0.65	287 (2.58)	1.86
ZrC	800*	1741	1.17	0.78	272 (2.45)	1.40
ZrC	1000*	1926	1.18	0.90	273 (2.45)	1.27
B_4C	600	1165	1.04	0.58	164 (1.47)	1.27
B_4C	750	1815			207 (1.86)	1.03
B_4C	800	2012	0.97	0.99	213 (1.91)	0.95
B_4C	1000	1857			196 (1.76)	0.95
B_4C	1200	1520	1.43	0.87	145 (1.30)	0.86
SiC	1100	1424	0.86	0.53	212 (1.91)	1.34
SiC	1200	1279	0.97	0.49	234 (2.10)	1.84

*Samples were hydrogen annealed at 600 ^{o}C for 2 h.

Available online at www.sciencedirect.com
SCIENCE DIRECT®
Microporous and Mesoporous Materials xxx (2005) xxx–xxx
MICROPOROUS AND MESOPOROUS MATERIALS
www.elsevier.com/locate/micromeso

Synthesis, structure and porosity analysis of microporous and mesoporous carbon derived from zirconium carbide

R.K. Dash *, G. Yushin, Y. Gogotsi

Drexel University, Department of Material Science and Engineering and A.J. Drexel Nanotechnology Institute, 3141 Chestnut Street, Philadelphia, PA 19104, USA

Received 20 January 2005; received in revised form 18 May 2005; accepted 31 May 2005

Abstract

Many applications of porous carbons demand control of pore size and its distribution. One of the most promising ways to mass-produce carbon with the desired porosity is by etching of non-carbon species from inorganic carbon containing materials, such as metal carbides. In this work, carbon was synthesized from zirconium carbide, $ZrC_{0.98}$, in a chlorine environment in the temperature range of 200–1200 °C. Thermodynamic simulation shows the possibility of carbon formation in a broad range of temperature. The structure of the resultant carbon analyzed using Raman spectroscopy, X-ray diffraction (XRD) and transmission electron microscopy (TEM), shows that ordering of carbon took place with increase in synthesis temperature. Porosity analyzed using gas sorption technique shows that carbon produced at low temperature (300–600 °C) has small pores with narrow pore size distribution; whereas carbon produced at high temperature (800–1200 °C) has large pores with wider pore size distribution. In comparison with other carbide derived carbons, B_4C and Ti_3SiC_2, whose pore size and its distribution do not change appreciably in 200–1000 °C range; carbon produced from ZrC can have both narrowly distributed micropores and mesopores depending upon the temperature of synthesis. As in carbons produced from other carbides, both the structure and porosity were found to depend on the synthesis temperature.

Keywords: Carbide derived carbon; Zirconium carbide; Argon sorption; Nanoporous carbon

1. Introduction

Highly porous carbons are in great demand because of their potential applications in gas storage, molecular sieves, catalyses, absorbents, electrodes in batteries and supercapacitors, water/air filters and medical devices [1]. For efficient application, a certain pore size distribution (PSD) is required in each case. Most porous carbons are produced through pyrolysis and activation of organic carbonaceous materials. However, this process does not allow the needed fine-tuning of the pore structure. Alternatively, carbons can be produced by extraction of metals from carbides. Such carbons are called carbide derived carbons (CDCs) [2]. Their structure and pore size can be tuned by choosing the appropriate synthesis conditions and the initial carbide [3,4]. In particular, it has been shown that PSD and specific surface area (SSA) of CDC derived from Ti_3SiC_2 [3] and B_4C [4] depend on the synthesis temperature. However, the effect of temperature on porous structure of CDC derived from other carbides has not been reported in literature.

Zirconium carbide is a commercially available transition metal carbide characterized by high hardness, high strength and high melting point. It has a face centered cubic (fcc) crystal structure (space group Fm3m) with a lattice parameter of 0.4698 nm and density of 6.59

* Corresponding author. Tel.: +1 2672306863; fax: +1 2158951934.
E-mail address: rkd25@drexel.edu (R.K. Dash).

1387-1811/$ - see front matter © 2005 Published by Elsevier Inc.
doi:10.1016/j.micromeso.2005.05.047

g/cc. Zirconium carbide is a non-stoichiometric carbide and its composition ranges from $ZrC_{0.55}$ to $ZrC_{0.99}$ [5]. As zirconium carbide crystallizes in a rock salt structure, with each zirconium atom surrounded by six carbon atoms at a distance of 0.2349 nm, the CDC produced at low temperature, where little structural rearrangement is allowed, is expected to have uniformly distributed small pores, similar to SiC-derived carbon [6]. Assuming the CDC reaction to be conformal (no shrinkage after metal extraction), simple theoretical calculation [2] shows that the ZrC-CDC should have a pore volume of 0.86 cc/g (66%) and a pore size of ~0.5 nm.

In this paper, we performed a systematic study of the effect of synthesis temperature on the structure and porosity of CDC synthesized from zirconium carbide (we will call it ZrC-CDC). Although formation of carbon upon chlorination of ZrC has already been reported in literature [7], little information is available on its PSD, and the effect of chlorination temperature on the porosity and structure of the resultant carbon.

2. Experimental

Zirconium carbide powder of chemical formula $ZrC_{0.98}$ was obtained from H.C. Stark. The starting material with the average particle size 8 μm contained 0.1% of free carbon with traces of oxygen, nitrogen, iron and hafnium.

The experimental setup for CDC synthesis was described elsewhere [2,4]. For etching of Zr from $ZrC_{0.98}$, the sample in a quartz boat was placed in a quartz tube furnace and heated to the desired temperature (200–1200 °C) under an argon (BOC Gases, 99.998%) purge. Once the desired temperature was reached, chlorine gas (BOC Gases, 99.5%) at a velocity of 10–15 cm^3/min was passed through the tube furnace (diameter = 1 in.) of tube furnace for 3 h. After the chlorination, the furnace was cooled down to room temperature under an argon purge.

Thermodynamic simulation was done using ChemSage v4.14 GTT advanced SOLGASMIX-based Gibbs energy minimization program. XRD analysis was done using a Rigaku diffractometer with CuK_α radiation ($\lambda = 0.154$ nm) operated at 30 mA and 40 kV. XRD patterns were collected using step scans, with a step size of 0.05° (2θ) and a count time of 2s per step between 10 and 60 (2θ). Samples were also analyzed by micro-Raman spectroscopy (Renishaw 1000) using an Ar ion laser (514.5 nm) at 500× magnification (~2 μm spot size). Deconvolution of the Raman spectra was done by using two bands: the D band and the G band of graphite with the peak fitting application provided by GRAMS software which uses an iterative fitting of Gaussian and Lorentzian functions with the data minimized by the chi-squared criterion. TEM samples were prepared by dispersing the sample in isopropyl alcohol over a copper grid with a lacey carbon film, TEM study was performed using JEOL 2010F microscope at 200 kV.

Sorption analysis of the porous carbon was done using Ar as adsorbate at −195.8 °C with Quantachrome Autosorb-1. The samples were degassed overnight under vacuum at 300 °C and backfilled with helium gas before the sorption measurement. The SSA of the porous carbon material was calculated for Ar sorption according to the BET (Brunauer, Emmet, Teller) equation [8–10]. PSDs and pore volume for Ar adsorption were calculated using the non-local density functional theory (NLDFT) method provided by Quantachrome's data reduction software (version 1.27) and developed by Neimark and co-workers [11].

3. Results

3.1. Thermodynamic simulation

Thermodynamic analysis of interaction between ZrC and Cl_2 was performed to understand the effect of temperature and chlorine amount in the system on the carbon formation. Fig. 1 shows thermodynamic simulation for the reaction of 1 mol of ZrC with 3 mol (Fig. 1a), 4 mol (Fig. 1b) and 5 mol (Fig. 1c) of Cl_2 in the temperature range of 0–1200 °C at a step of 50 °C. The calculations were performed for a closed system with a total constant pressure of 1 atm. The simulations resulted in three chemical equations for three different temperature ranges.

Range I: In this low temperature range, no CDC synthesis is thermodynamically possible under equilibrium conditions due to the preferential formation of CCl_4 over solid C, as shown in following reaction:

$$ZrC_{(s)} + 4Cl_{2(g)} \rightarrow ZrCl_{4(s,g)} + CCl_{4(s,g)} \quad (1)$$

Range II: In this mid temperature range, CDC forms and its amount increases with temperature. However, the carbon yield is still limited by the formation of CCl_4.

$$ZrC_{(s)} + 3Cl_{2(g)} \rightarrow ZrCl_{4(s,g)} + 0.5C_{(s)} + 0.5CCl_{4(s,g)} \quad (2)$$

Range III: In this high temperature range, there is no formation of $CCl_{4(s,g)}$ and thus there is no loss of carbon as $CCl_{4(s,g)}$ which results in the formation of 1 mol of carbon per mol of carbide.

$$ZrC_{(s)} + 2Cl_{2(g)} \rightarrow ZrCl_{4(g)} + C_{(s)} \quad (3)$$

The temperature limits of each range depend on the amount of Cl_2 used in the calculation. Range II, for example, changed from ~0–600 °C to ~250–700 °C and to ~350–750 °C when the amount of Cl_2 changed

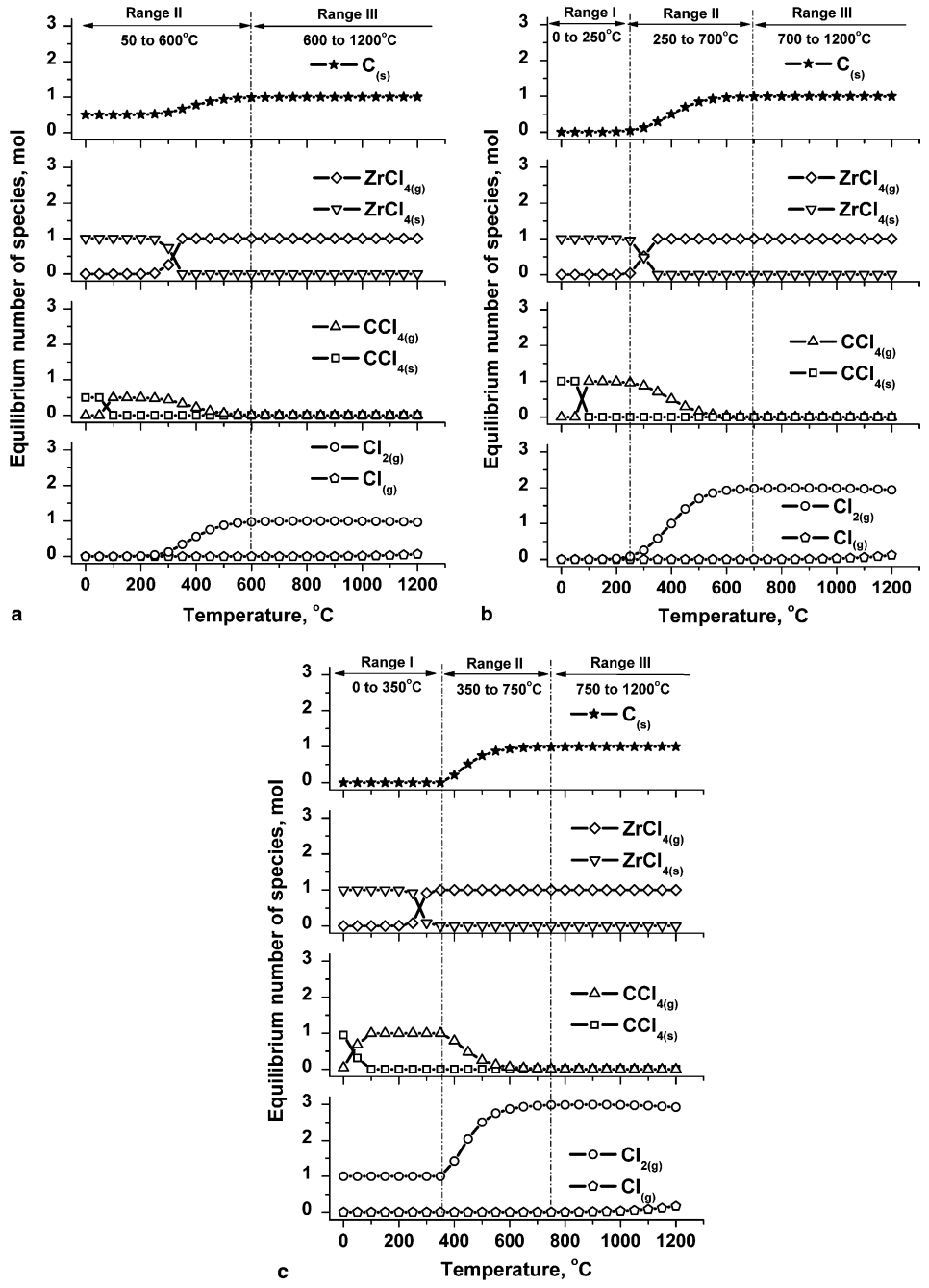

Fig. 1. Equilibrium reaction products as a function of chlorination temperature for 1 mol of ZrC and with (a) 3 mol, (b) 4 mol and (c) 5 mol of Cl_2.

from 3 to 4 and to 5 mol, respectively, while the amount of ZrC was kept constant (1 mol). Thus, decreasing chlorine concentration favors formation of carbon, while excess chlorine may etch carbon, eventually leading to a lower yield and/or larger pore size.

As the chlorination experiments were performed in an open environment, the results of the performed simulations provided only general guidelines for the experimental design and were not expected to give precise quantitative information.

3.2. Powder XRD

XRD analysis was carried out on powder samples to investigate the structural changes in ZrC-CDC that occurred at different chlorination temperatures. The XRD patterns (Fig. 2) of CDC produced at 200 °C showed peaks of ZrC, suggesting the incomplete conversion of ZrC to CDC. At temperatures of 300 °C and above, only two peaks, corresponding to the (002) and (004) planes of graphite were seen. The large width

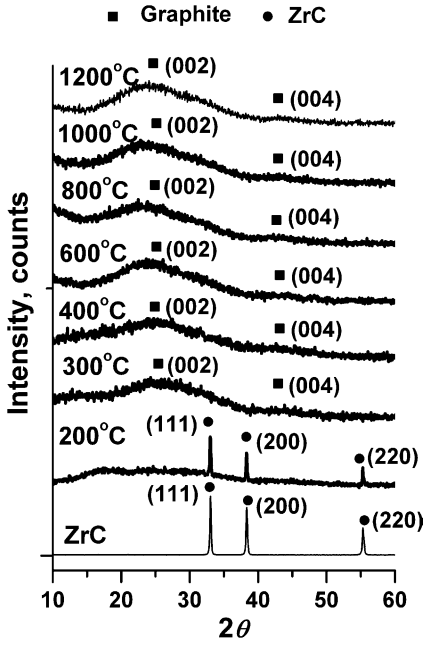

Fig. 2. XRD of untreated ZrC and samples chlorinated at different temperatures.

of these peaks suggested a disordered structure of the CDC formed in this temperature range. As temperature increased from 300 to 1200 °C, the peak became more narrow indicating ordering of carbon.

3.3. Raman spectroscopy analysis

The first-order Raman spectra of perfectly ordered graphite only show one peak at 1582 cm^{-1}, whereas the disordered carbon generally demonstrates two peaks: the graphite (G) peak at ~1582 cm^{-1} and the disorder-induced (D) peak at ~1350 cm^{-1} [12,13]. Another disorder-induced peak (the D′ peak) located at ~1600–1620 cm^{-1} [12,13] is often superimposed with the broad G peak in disordered carbons and thus is not considered separately. G peak corresponds to in-plane stretching of graphite [14,15] whereas the D-peak is generally associated with a double-resonance Raman process in disordered carbon [16]. The D′-peak corresponds to a strong maximum in the vibrational density of states (VDOS) of graphite [12].

Raman spectra of the as-received zirconium carbide sample showed very weak D and G bands indicating traces of free carbon. As the temperature of synthesis increased from 200 to 1200 °C, CDC becomes more ordered as evident by a decrease in full width at half maximum (FWHM) values of the D-band and G-band of graphite (Figs. 3 and 4a). At 1200 °C, the FWHM of D and G bands were ~80 and 90 cm^{-1} which is about 5 times the value of graphite single crystal. As in most CDCs [3,17], the ratio of the integrated intensities of D and G bands (I_D/I_G) decreases with synthesis temper-

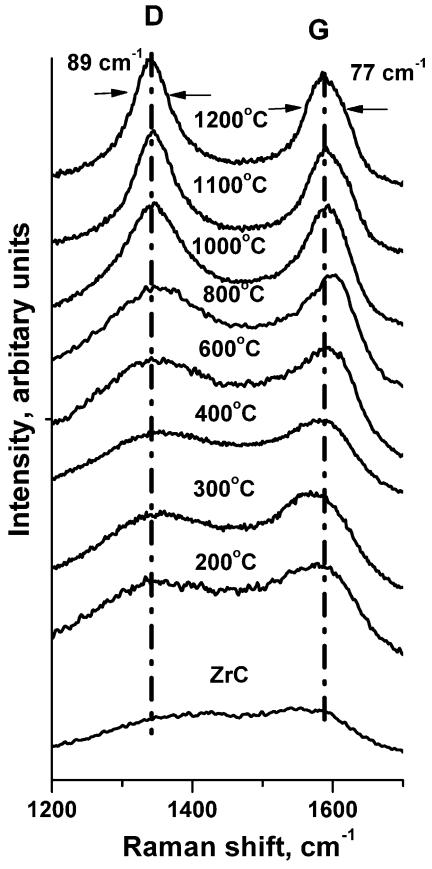

Fig. 3. Raman spectra of untreated ZrC and samples chlorinated at different temperatures.

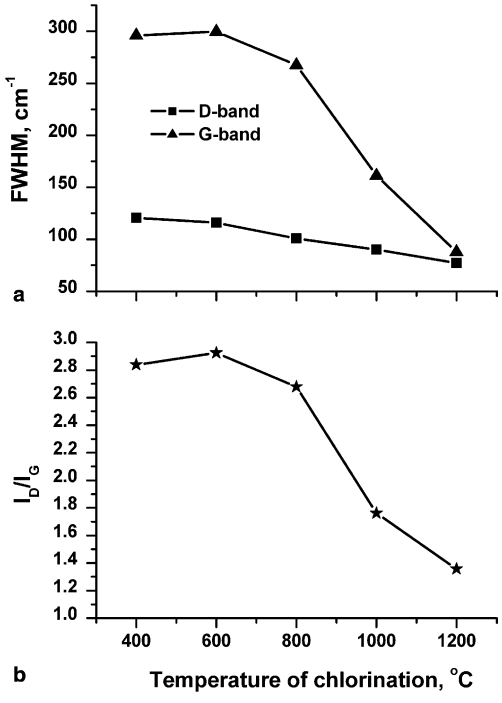

Fig. 4. Raman analysis of ZrC-CDC. (a) FWHM of D and G bands and (b) I_D/I_G ratio for different temperatures of chlorination.

ature, which is probably due to the formation of planar graphite at high temperature (Fig. 4b).

3.4. TEM analysis

In agreement with XRD and Raman spectroscopy, TEM revealed an increase in the degree of ordering in the CDC with chlorination temperature. At 300 °C, the CDC produced consisted of amorphous carbon (Fig. 5a). At 800 °C, along with the presence of amorphous carbon, the formation of thin graphitic ribbons (Fig. 5b) was seen. At 1200 °C (Fig. 5c), CDC contained less amorphous carbon and more ordered curved sheets of graphite with an interplanar distance of ~0.34 nm, which is slightly higher than the interplanar spacing of (0002) planes of graphite (0.335 nm). The average thickness of graphite ribbons was less than 1 nm. It was noticed however, that the edges of the CDC particles contain thicker ribbons.

At low chlorination temperatures, the diffusion of carbon atoms is extremely slow and they are only slightly displaced from their original positions in the ZrC lattice, leading to the amorphous structure. As synthesis temperature increased, the diffusion rate of carbon atoms increased allowing them to arrange themselves in more ordered carbon structures. The diffusion of surface carbon atoms is easier and thus the formation of graphite layer will first take place at the surface of ZrC grains. It is also important that since extraction starts from the surface, the surface carbon atoms may experience rearrangement due to diffusion and gas phase transport while the reaction propagates towards the center of the particle.

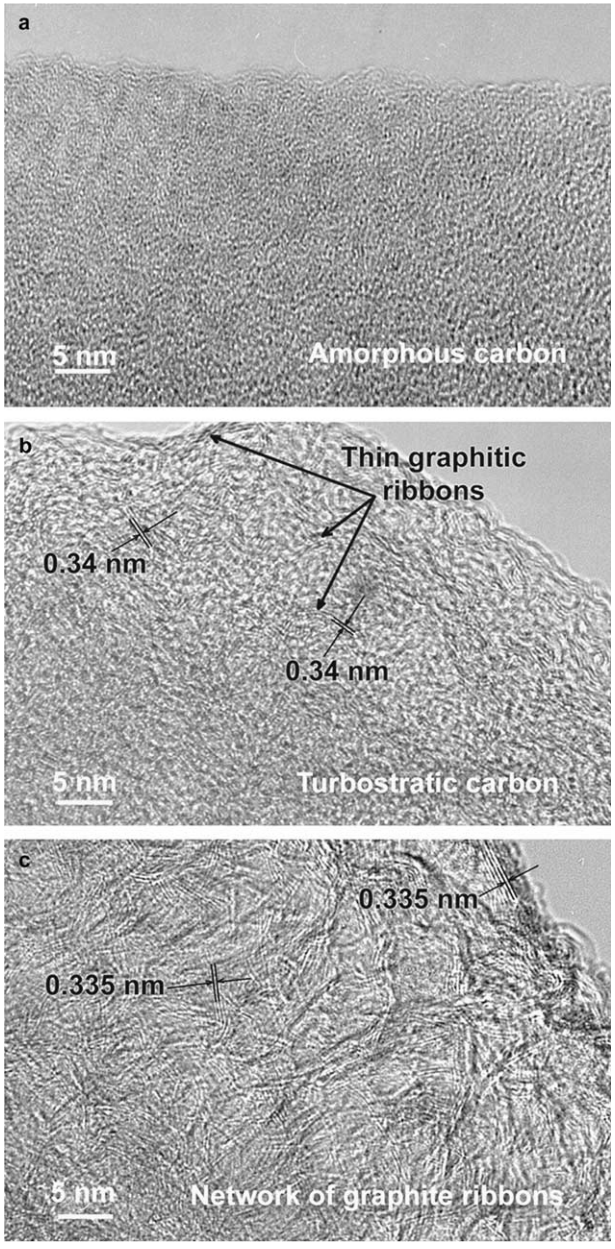

Fig. 5. TEM images of CDC produced from ZrC at temperatures of (a) 300 °C, (b) 800 °C and (c) 1200 °C.

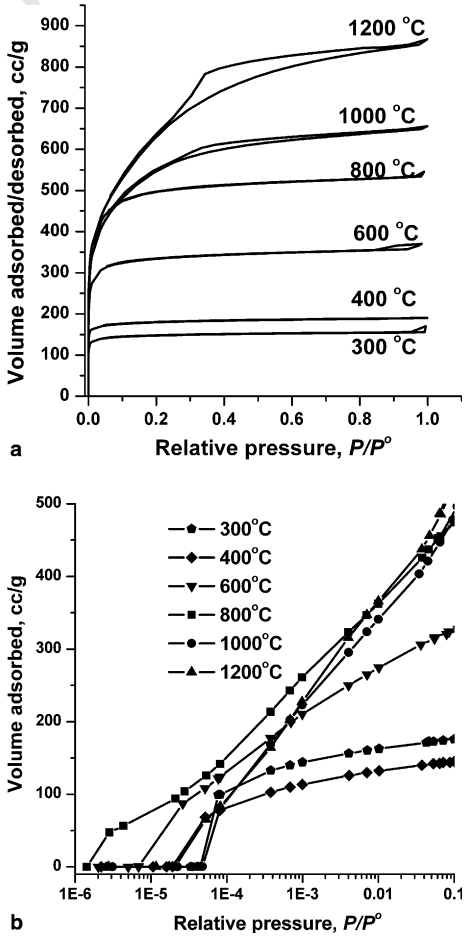

Fig. 6. Argon adsorption and desorption isotherm at −195.8 °C of CDC derived from ZrC at different temperatures: (a) whole isotherm at a linear relative pressure scale; (b) semilogarithmic scale plot showing the low pressure part of the diagram in (a).

3.5. Argon sorption analysis

Porosity analysis was carried out on samples chlorinated at 300, 400, 600, 800, 1000 and 1200 °C using of Ar as the absorbate and liquid nitrogen as the coolant. The SSAs of the completely converted CDC samples were calculated using the BET equation for volume of gas adsorbed at relative pressures between 0.05 and 0.3, where the BET isotherm is linear. Isotherms of 300–800 °C samples (Fig. 6a) belong to type-I [18] of the Brunauer classifications [19], which is a characteristic of microporous materials (pore size less than 2 nm according to IUPAC classification). A small hysterisis loop in the adsorption–desorption isotherm of the 1000 °C sample was seen between a relative pressure of 0.3 and 0.9. This hysterisis loop significantly widened for the sample synthesized at 1200 °C.

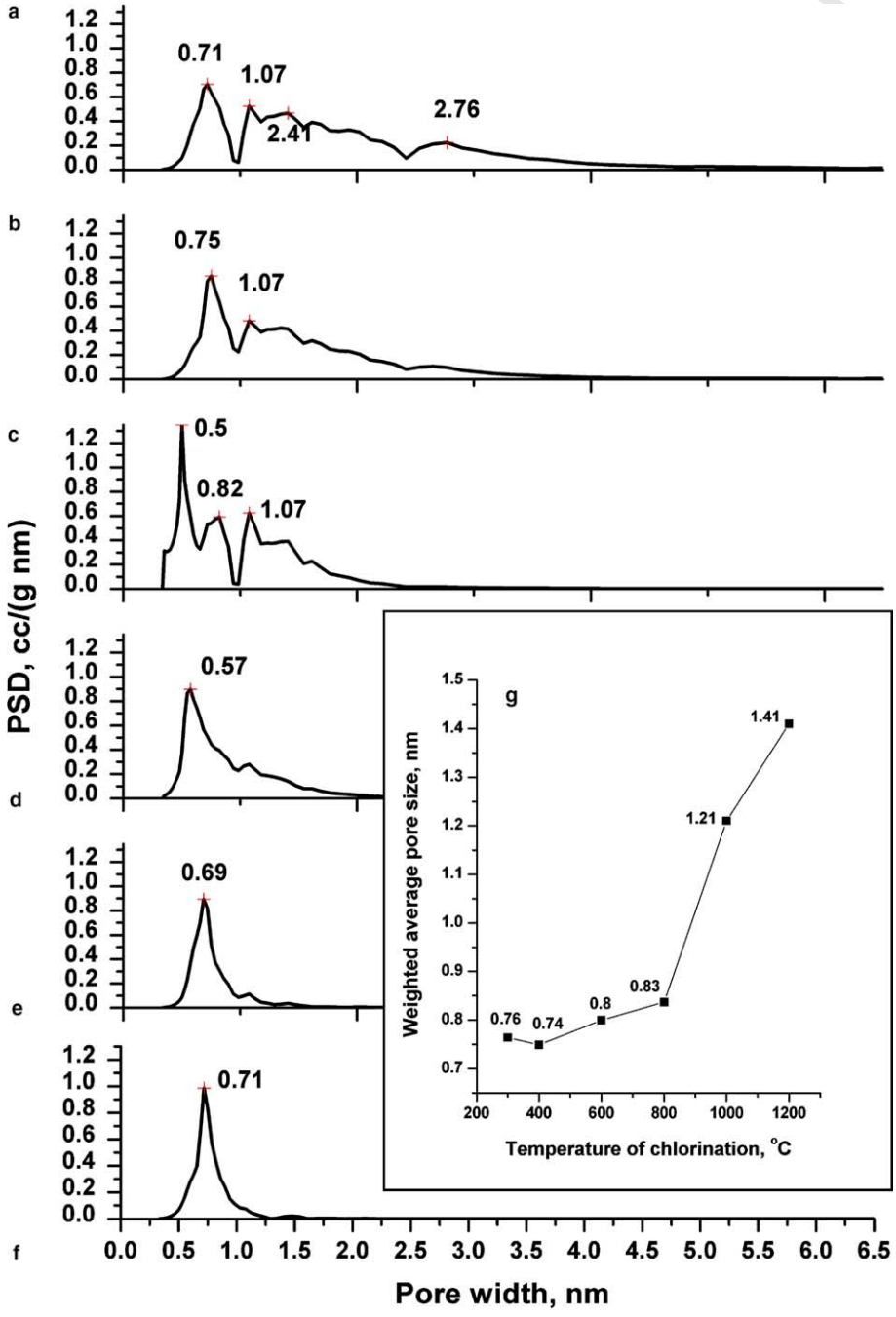

Fig. 7. Pore size distributions for CDC derived from ZrC at temperatures of (a) 1200 °C, (b) 1000 °C, (c) 800 °C, (d) 600 °C, (e) 400 °C and (f) 300 °C. Distributions were calculated for argon adsorption at liquid nitrogen temperature using NLDFT method; (g) D_0 (weighted average pore size) for CDC derived from ZrC at various temperatures.

A semilogarithmic scale plot of the argon isotherms in Fig. 6b allows one to differentiate between the sorption behaviors of the samples at low pressures. The 800 °C ZrC-CDC sample adsorbs more Ar at a relative pressure between 10^{-6} and 10^{-5} than ZrC-CDC prepared at any other temperature suggesting that this material has smaller pores than any other ZrC-CDC sample synthesized. Similarly, the 600 °C sample possess pores larger than that of the 800 °C sample but smaller than that of the other CDCs.

The SSA increased with chlorination temperature from ~500 m^2/g at 300 °C to a maximum of ~1900 m^2/g at 1200 °C (Fig. 7b). The total pore volume also showed gradual increase from ~0.2 cc/g at 300 °C to over 0.9 cc/g at 1200 °C. The high values of pore volume achieved at high temperature (higher than the theoretical pore volume of 0.86 cc/g) indicates partial etching of carbon due to uncontrolled oxidation by traces of oxygen or formation of CCl_4. Interestingly, the volume of micropores did not show significant changes at temperatures above 600 °C whereas the mesoporous volume increased significantly from less than 0.04 cc/g at 300 °C to 0.46 cc/g at 1200 °C.

Fig. 8 shows PSDs of CDCs calculated using the NLDFT method assuming slit shaped pores. Although the real shape of the pores is not known, the slit pore assumption seemed reasonable as previously produced CDC derived from Ti_3SiC_2 showed slit shaped pores according to the small angle X-ray scattering analysis [3]. In contrast to classical thermodynamic methods for calculation of PSDs, the NLDFT method is based on a statistical mechanics model, and calculations depend on the absorbate–absorbent system. The statistical mechanical model used in NLDFT can be described as the best fit obtained by comparing the theoretical isotherms for argon sorption on carbon to the experimental data. The filling of micropores occurs in a continuous way whereas the filling of mesopores occurs by pore condensation, which represents a first order transition from a gas-like state to a liquid-like state. Classical thermodynamic theories like Barrett–Joiner–Halenda (BJH) are based on pore condensation and thus are only applicable to mesopores. Dubinin–Radushkevich (DR), Horvath and Kawazoe (HK), and Saito and Foley (SF) methods are based on continuous pore filling and thus are applicable to micropores only [11,20]. For a material having both micropores and mesopores, the above-mentioned methods cannot accurately describe PSDs and thus we took NLDFT as a method of choice for ZrC-CDC samples. The PSDs of 300, 400 and 600 °C samples were narrow with D_m (pore size corresponding to the maximum in PSD) equal to 0.71, 0.69 and 0.57 nm, respectively where as the PSDs of 800, 1000 and 1200 °C samples were wide. The weighted average pore size, D_0 for various chlorination temperatures (Fig. 7g) shows that the pore size increases with chlorination temperature. However, a decrease of D_m with increasing temperature to 800 °C suggests that pore structure evolves by short range transport of carbon. When a wall between two cells (pores) of equal size shifts a pore of a smaller size and a larger pore appear. This can explain the transition from a narrow PSD at 300 °C to a wide PSD at 600 °C.

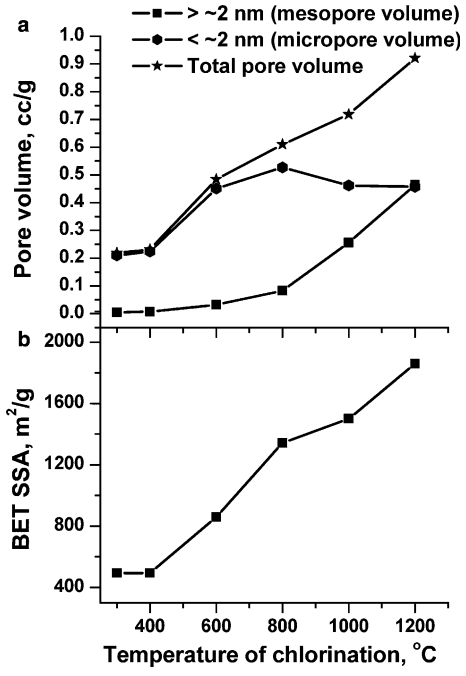

Fig. 8. Results of Ar sorption analysis of CDC-ZrC. (a) Pore volume and (b) BET SSA as a function of the temperatures of chlorination.

4. Discussion

At low synthesis temperatures, the diffusion of carbon is slow and the morphology of the carbon network formed is expected to be close to the distribution of carbon atoms in the initial carbide structure. As discussed, a porosity of 66% was expected for the ZrC-CDC synthesized. The low SSA in samples produced at low temperature showed that some pores might be blocked by Cl_2 and $ZrCl_4$ remaining in the CDC.

Similar to what we observed in other studies [3], structure of porous amorphous CDC showed small pores and narrow PSDs. Such CDCs are generally synthesized at low temperatures (below 600 °C in the present case). As the temperature increased to 800 °C and above, the ordering of amorphous carbon took place, as was evident from Raman and TEM analysis, and PSDs widened. The formation of multi-layer graphitic structures at higher temperatures resulted in the increase of the weighed average pore size (D_0). Although loss of carbon atoms (due to the accidental oxidation or the formation of gaseous CCl_4) or incomplete removal of

chlorine or chlorides may alter the obtained PSD, the discussed dependence of D_0 is accurate and was observed in all of our studies. The previously discussed increase in mesoporous volume at higher temperatures can be explained by the growth of graphitic ribbons observed by TEM. Ar sorption analysis of ZrC-CDC samples showed that the SSA increased with temperature and the corresponding Raman and XRD analysis indicated that ordering of carbon is not because of densification. The increase of SSA with temperature also indicates that most of the pores formed in the CDC at high temperature are open and large enough to be accessible to Ar. The absence of a strong and narrow graphitic peak in Raman spectra indicated that the formed ribbons are highly defective (turbostratic) and thus may adsorb more Ar than thin graphite sheets of comparable wall thickness. The surface area of CDC increases with temperature and reaches $>2000\ m^2/g$ at 1200 °C.

In comparison to CDCs produced from B_4C [4] and Ti_3SiC_2 [3], whore PSDs do not change appreciably in 200–1200 °C range, CDC produced from ZrC can have both narrowly distributed micropores and mesopores depending upon the temperature of synthesis. However, the PSD is significantly broader than in case of SiC-CDC.

ZrC-CDC produced at low temperature can be an excellent candidate for gas storage and molecular sieves, while ZrC-CDC produced at higher temperatures (800 °C and above) may find applications in sorbents, batteries and supercapacitors.

5. Conclusions

Highly porous carbon was synthesized by chlorination of ZrC at different temperatures. Thermodynamic analysis predicts formation of CCl_4 below 250–400 °C, depending on amount of chlorine in the system. One mole of carbon and $ZrCl_4$ are predicted above 400 °C. XRD, micro-Raman spectroscopy, and TEM showed that the carbon was amorphous to 600 °C, 2–3 layer graphite ribbons were observed at higher temperatures. Argon sorption measurements show that the porosity of the CDCs depends on the chlorination temperature. At low temperatures (below 600 °C), the material contained small pores with a narrow PSD whereas at high temperature (above 1000 °C), the material contained larger pores with broad PSD. In comparison to CDCs produced from B_4C [4], Fe_3C [17] and Ti_3SiC_2 [3], the ZrC-CDC shows a lower degree of ordering at high temperatures. In comparison to CDCs produced from B_4C [4] and Ti_3SiC_2 [3], whose PSDs do not change appreciably in 200–1000 °C range, CDCs produced from ZrC can have both narrowly distributed micropores and mesopores depending upon the temperature of synthesis. However, the PSD is significantly broader than in case of SiC-CDC.

Acknowledgments

This work was supported in part by Arkema Inc. The purchase of the Raman spectrometer was supported by NSF grants DMR-0115546 and BES-0216343. HRTEM and XRD were performed in the Regional Materials Characterization Facility at the University of Pennsylvania.

References

[1] F. Schuth, S.W.K. Sing, J. Weitkamp, Handbook of Porous Solids, 3, WILEY-VCH, 2002.
[2] A. Nikitin, Y. Gogotsi, in: H.S. Nalwa (Ed.), Nanostructured Carbide-Derived Carbon (CDC), Encyclopedia of Nanoscience and Nanotechnology, vol. 7, American Scientific Publishers, CA, 2003, p. 553.
[3] Y. Gogotsi, A. Nikitin, H. Ye, W. Zhou, J.E. Fischer, B. Yi, H.C. Foley, M.W. Barsoum, Nat. Mater. 2 (2003) 591.
[4] R.K. Dash, A. Nikitin, Y. Gogotsi, Micropor. Mesopor. Mater. 72 (2004) 203.
[5] H.O. Pierson, Handbook of Refractory Carbides and Nitrides, William Andrew Publishing/Noyes, 1996.
[6] Y. Gogotsi, V.L. Kuznetsov, G.N. Yushin, A. Nikitin, A.V. Okotrub, A.I. Romanenko, A.I. Boronin, E. Pozhetnov, Carbon (2005).
[7] V.P. Orekhov, G.V. Seryakov, A.N. Zelikman, T.M. Starobina, T.I. Kahzanova, K.V. Petrova, P.M. Sverchkov, J. Appl. Chem. USSR 42 (1969) 230.
[8] S. Brunauer, P. Emmett, E. Teller, J. Am. Chem. Soc. 60 (1938) 309.
[9] S.J. Gregg, K.S.W. Sing, Adsorption, Surface Area and Porosity, Academic Press, London, 1982.
[10] S. Lowell, J.E. Schields, Powder Surface Area and Porosity, New York, 1998.
[11] P.I. Ravikovitch, A.V. Neimark, Colloids Surf. 187–188 (2001) 11.
[12] R.J. Nemanich, S.A. Solin, Phys. Rev. B 20 (1979) 392.
[13] R.P. Vidano, D.B. Fishbach, L.J. Willis, T.M. Loehr, Solid State Commun. 39 (1981) 341.
[14] R.J. Nemanich, G. Lukovsky, S.A. Solin, in: M. Balkanski (Ed.), Proc. Int. Conf. Lattice Dyn., Flammarion Press, Paris, 1975, p. 619.
[15] F. Tuinstra, J.L. Koenig, J. Chem. Phys. 53 (1970) 1126.
[16] C. Thomsen, S. Reich, Phys. Rev. Lett. 85 (2000) 5214.
[17] S. Dimovski, A. Nikitin, H. Ye, Y. Gogotsi, J. Mater. Chem 14 (2003) 238.
[18] H. Takikawa, R. Miyano, M. Yatsuki, T. Sakakibara, Jpn. J. Appl. Phys. 37 (1998) L187.
[19] P.A. Webb, C. Orr, Analytical Methods in Fine Particle Technology, Micromeritics Instrument Corporation (1997).
[20] J. Jagiello, M. Thommes, Carbon 42 (2004) 1227.